Assessing 3D morphological dune changes using medial axes

Roderik LINDENBERGH[1,*], **Thomas DEWEZ**[2], and **Daan HULSKEMPER**[1]

[1] *Dept. of Geoscience and Remote Sensing, Delft University of Technology, Delft, The Netherlands, (r.c.lindenbergh, d.c.hulskemper@tudelft.nl)*

[2] *BRGM: French geological survey, Orléans, France, (t.dewez@brgm.fr)*

[*] *corresponding author*

Abstract

Representing and characterizing terrain change dynamics from multi-epoch 3D point clouds remains a challenge. In case of 2 epochs, subtracting the corresponding terrain models conveys local erosion and sedimentation patterns, but not landform rotation and translation. Current laser scanning possibilities provide us easily with 10s (drone or airplane based LiDAR) to 1000s (permanent laser scanning) of consecutive epochs of terrain data representing sandy beach-dune systems. Coastal dunes grow or shrink vertically over time, but also migrate and reorient due to eolian or marine forcing. Instead of considering pairwise epoch comparisons, we propose to assess the change of such dynamic 3D objects by simplifying these objects using the so-called medial axis transform (MAT) as shape descriptor. The MAT provides MAT points that are positioned centrally inside (or outside) the surface, here the dune surface as sampled by laser scanning. The MAT points can directly or indirectly, via a local neighborhood analysis, be used to estimate local dune ridge positions. The MAT radius is a parameter directly linked to the local scale of a dune. The MAT analysis also allows to estimate the local orientation and asymmetry of the considered dunes. This MAT methodology will be demonstrated on 2 different case studies. The first case considers 5 epochs of UAV-LiDAR data of an embryo dune field at the Sand Engine, The Netherlands. The second case considers a mature dune system sampled by 3 epochs of airborne LiDAR data, i.e. the Dune du Pila on the French Atlantic coast.

Keywords: 4D, deformation analysis, laser scanning, morpho-dynamic

1 Introduction

Multi-epoch 3D point clouds are increasingly used in geomorphology with the hope that measuring the state and rates of morphological changes will help flag the processes behind these topographic changes. With the rise of ever easier topographic acquisition devices, point clouds come in time series of tens to thousands. As a consequence, making sense of the spatio-temporal vertical change pattern becomes increasingly difficult. Current attempts to extract meaning from point cloud sequences has focused on detecting regions where points change in a similar fashion both in elevation and time (Kuschnerus et al., 2021). A search for causal processes is then launched to explain the temporal sequences of the different geographic clusters (Hulskemper et al., 2022).

An alternative approach is object-based change detection. In each epoch, objects are detected, then matched across epochs, and finally geometric changes in object parameters are reported. In geomorphology, these objects are the landform under consideration. Key for an object-based approach is to determine, first, what characterizes a particular type of landform, and, second, how such character can be expressed as a descriptor that can be effectively extracted from detailed unstructured 3D point clouds.

In case of dunes and dune fields (Grohmann et al., 2020), the objects are individual dunes and compositions thereof. Geomorphologists analyzing dunes may retain their height, volume, orientation and shape or regularity (Walker et al., 2013). For a single, isolated dune, this may come down to analyzing its outline and ridge line. Recently, Daynac et al. (2024) presented a workflow to, first, identify dune fields using deep learning from DEM-derived images, and second, to extract ridges and outlines from the DEM represented as a gray scale image through a morphological surface skeletonization approach. Chen et al. (2023) uses surface skeletons to reconstruct terrain in an alternative deep learning approach.

Above methods extract line elements from 2.5D raster representations of dune terrains. An alternative approach is to describe dune geometric structure natively in 3D, first, above and below the topographic surface over a range of spatial scales, and, second, to use this structural description to explore the geomorphological properties of the dune. The structural descriptor is the medial axis transform skeletonization method. The medial axis of a 2D or 3D object is defined as the locus, i.e., the collection of points in the containing space that are at equal closest distance to two points on the surface of an object. In addition to the location of the medial axis points itself, their distance to the topographic surface also informs the object shape. The extraction of both medial axis points and associated radius is referred to as Medial Axis Transform (MAT), Blum (1967). The notion of MAT is closely related to those of center line and skeleton. One difference though is that the MAT of a 3D object is not necessarily built up from line elements.

In recent years robust algorithms have been developed to extract the medial axis in 3D, from noisy, real world point clouds. Peters and Ledoux (2016) showed how to extract the MAT from noisy airborne laser scanning point clouds, for visualization purposes. Widyaningrum et al. (2020) shows how the MAT can be used in extracting building outlines from airborne laser scanning point cloud. However MAT has hardly been exploited for 3D geomorphological monitoring applications. Therefore the goal of this contribution is as follows:

- Use MAT and its properties to parameterize dune shape in different settings, from sets of LiDAR point clouds.
- Explore the potential of MAT and its properties in characterizing dynamic dune changes.

These goals mean to design a single epoch cloud-to-features algorithm, and then look for feature sequence dynamics descriptors. Skeleton pattern development is expected to relate to eolian forcing and may offer a means of predicting the future state and size of beach features. Presumably, sand flux will be highest when dunes/shoals are fully expressed and reduced when in transition state.

2 Methodology: medial axis

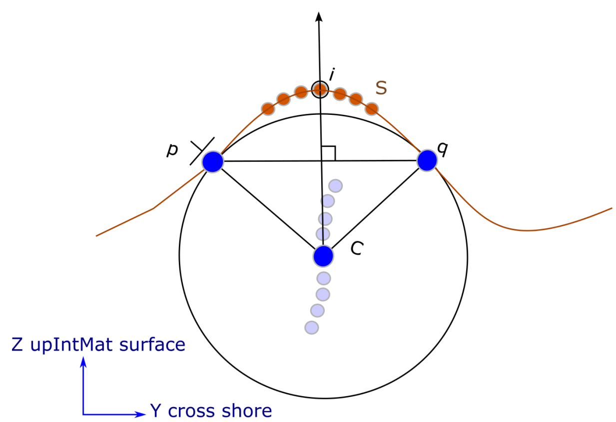

Figure 1. Medial axis point c is the center of the medial ball touching the surface S in points p and q.

2.1 Definition of medial axis

Suppose we are given a set of 3D surface points S. A point c is part of the medial axis M_S of S if there exists an empty sphere, centered at c that touches S in two points, and contains no points of S in its interior, compare Figure 1. Note that each medial axis point c comes with a radius ρ_c of its defining empty sphere. The larger this radius ρ_c, the further c is from the surface S, which gives a sense of scale of the surface it corresponds to. Smaller spheres describe narrow ridges, while larger spheres fit more open hills. The collection $\{c_S\}$ of sphere centers progressively fitting ridge sections will form a line in 2D, and a surface in 3D. The shape of this 3D surface summarizes characteristics of the landscapes : presence of a curved surfaces, their aperture (pcq angle), and their asymmetry.

The medial axis is defined for either side of the surface S. In the context of dunes, parts of the medial axis corresponding to its ridges, will be below the surface (i.e., the internal MAT), while the parts of the medial axis corresponding to dune toes or heels will be above the surface (i.e., the external MAT). In Figure 1 only the part of the medial axis below the surface is shown. Peters and Ledoux (2016) defines the Medial Axis Transform (MAT) as the set of medial spheres, and the medial axis as the set of medial sphere centers.

2.2 The MAT algorithm

An efficient way to compute an approximation of the MAT is described in Peters and Ledoux (2016) and extends the so-called shrinking ball algorithm (Ma et al., 2012). The input is a set of 3D points on an oriented surface, which means that each point possesses a pre-computed normal vector pointing outward of the surface S. At each point p belonging to surface S, a large sphere is fitted. The sphere surface is tangent to surface S (meaning vector cp is collinear with the normal in p). This sphere radius is progressively reduced until only one other point of S, q, touches the sphere surface and no other point of S remains inside the sphere. As the fitting algorithm is sensitive to measurement noise, Peters and Ledoux (2016) implemented two additional checks that favors more robust MAT results.

2.3 MAT parameters

To run the MAT algorithm, some parameters need to be set. For the initial MAT algorithm these are the **radius** of the initial large sphere and a **neighborhood size** to estimate a surface normal from points within the neighborhood. For the robust extension, two additional parameters are needed. First, a **denoising parameter**. The idea is, compare Figure 1, that if a ball is spanned between initial point p, center point c, and point q, the separation angle $\angle pcq$ should not be smaller than a given threshold. If it is, this might be the result of some random error around the actual surface. If this angle is below the threshold after a shrinking iteration, the previous ball (and center) are used instead as final MAT center. The second extension considers the **surface planarity**. Planar surfaces have an infinite curvature radius.

If at the first iteration the angle $\angle pcq$ is smaller than the **planarity parameter** threshold, the procedure is stopped and we do not look for a MAT for surface point p under consideration, as p in this case is apparently part of a near-planar surface, which would correspond to a near-infinite MAT radius.

2.4 MAT based ridge extraction

Because the vector cp is collinear with the surface normal, internal MAT sphere centers are located below the topographic surface. The ridge line does not belong to the MAT. An approximate ridge location is obtained by extrapolating the trend of the MAT

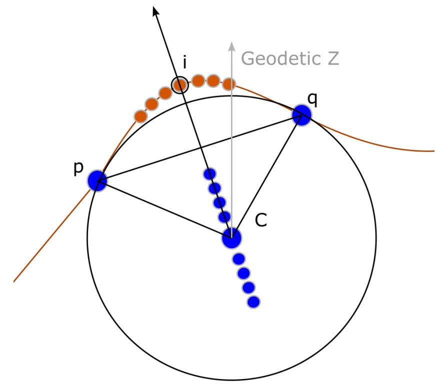

Figure 2. MAT points (in blue) around given MAT point c are used to estimate local dune dip direction. The dip direction vector intersects the surface S in approximate ridge point j.

surface across the topographic surface, see Figure 2. The ridge point is the nearest surface point i to the medial vector c_i. Vector c_i is collinear with the trend of the MAT surface. This trend is locally orthogonal to the MAT surface normal. We solve it empirically by rotating the topographic point cloud reference frame to the dominant dip/direction of the MAT surface and project along the pseudo coordinate axis Z. Ridge line points lie in the direct neighborhood of projected centers c.

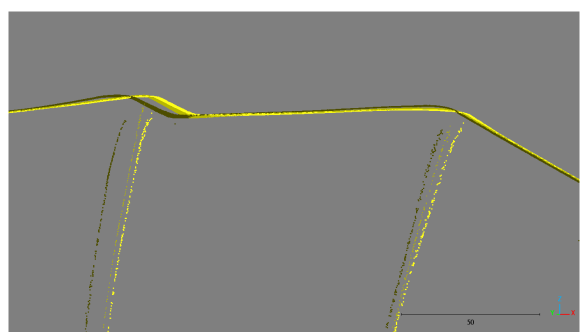

Figure 3. Cross section through successive topographic epochs $P1$ to $P3$ and corresponding inclined MAT surfaces. The ocean is on the left (West), land is on the right (East). MAT inclination to the right indicates dominance in shaping the sand pile.

This projection approach is only precise if the MAT surface is planar upward. With complex dunes, the MAT surface is curved in 3D and the average dip/dip-direction approximation may slightly inaccurately flag topographic points as ridge lines, compare Figure 3. Further development is required to solve this labeling in a more satisfying way.

In the case of symmetrical dunes, a simplification of the method is used. In this case, the MAT surfaces are expected to be approximately vertical. As a consequence, ridge points lie directly above MAT sphere centers. In other words, the ridge positions are directly indicated by the xy coordinates of the MAT points. Capturing ridge line migration is one of our goals. We will show that the MAT method indeed retrieves this indicator of dune dynamics from a point cloud sequence. Dune asymmetry relates to force imbalance between morphogenic processes. In Figure 3, windblown ridge lines display this imbalance between gravity and a westerly wind - acting from the left of the figure.

2.5 Descriptive MAT parameters

In addition to the ridge points, other MAT parameters also have a direct morphological interpretation. The local **MAT radius** quantifies dune size and kurtosis. Larger dunes will have in general bigger local MAT radius as the dune surface would fit a larger empty MAT sphere. If a dune hosts superimposed narrower ridges and ripples, these will be fitted by shorter radii. A complete MAT surface therefore captures the whole range of morphological feature's length-scales at once. The **MAT dip direction**, equivalent to the MAT-normal azimuth, can also be directly estimated from a local neighborhood of MAT points, see Figure 2. It gives the local ridge normal and relates to the forces acting to alter it shape. The **MAT dip**, i.e., the 1D slope of the planes approximating the MAT neighbors of a MAT point c is an indication for the local asymmetry of the dune. A strictly horizontal MAT dip of 90° would describe a symmetrical section, with p and q at equal elevation and a strictly vertical vector c_i. An oblique dip (less than 90°) indicates an asymmetry between ridge limbs, and thus an imbalance between morphogenic forcing, i.e., gravity vs. dominant wind transport.

2.6 Implementation

Results in this paper were extracted and visualized using Python and CloudCompare. The robust MAT algorithm by Ravi Peters was used, as described in Peters and Ledoux (2016). His code is available via (Peters, 2018).

3 Data description

Table 1. LiDAR acquisition dates, for Sand engine (left) & Pila (right)

Epoch	Date	Epoch	Date
S1	27-2-2024	P1	23-7-2023
S2	1-5-2024	P2	3-9-2023
S3	7-6-2024	P3	30-9-2023
S4	17-7-2024		
S5	9-10-2024		

Methodology is demonstrated on two different LiDAR data sets, see Table 1. First, on five epochs of UAV LiDAR data of a field of juvenile dunes at the Sand engine in The Netherlands, and, second, on three epochs of aerial LiDAR data of the large French Dune du Pila.

Figure 4. Embryo dunes at the Sand Engine (Photo: W. van Teeffelen)

3.1 UAV LiDAR data - Sand engine

The Sand engine, just South of the Dutch city of The Hague is a large sand suppletion project that resulted in a sandy peninsula of ~ 10 km^2 directly on the coast. It started ~ 10 years ago and shows a variety of dynamic processes (Stive et al., 2013). Notably an embryonic dune field emerged, see Figure 4, consisting of juvenile dunes of a few meters high, typically consolidated by marram grass.UAV LiDAR data of the dune field has been acquired in five epochs, S1 to S5, by a Yellowscan Mapper+ system with a point density of about $300 pts/m^2$ between February and October 2024. A first impression of the dynamics of the area is presented in Figure 5.

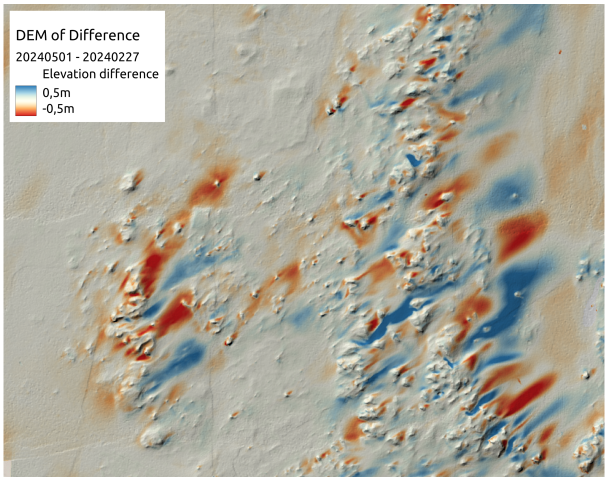

Figure 5. Flared spatially intermittent erosion/accretion patterns between UAV LiDAR epochs $S1$ and $S2$ at the Sand engine.

The figure shows a plot of the differences between epochs S1 and S2, which were acquired 2024-02-27 and 2024-05-01, respectively. This image shows the spatial correlation between small dunes and the erosion/ deposition pattern.

To speed up MAT computation, point clouds were rasterized from nominal $300 pts/m^2$ to regular 0.25 m grid pixels using an ordinary mean of all cell points.

3.2 ALS data - Pila

Dune du Pila on the French Atlantic coast is part of the largest coastal sand dunes in the world. It reaches a height of over 100 m (Bossard and Nicolae Lerma, 2020). LidarHD flew several times over the dune in 2023, see dates in Table 1. Classified point clouds are available from IGN (2025). The final point density reached 60 pts/m^2 (distribution mode) in tile 0365-6387, cf. Figure 8, by stacking three distinct campaigns, over the course of 67 days. This practice unwillingly captured the highly dynamic nature of the dune all bundled in a single LAZ file. In this work, all three epochs, $P1$ to $P3$ are processed, see Table 1. The point clouds were rasterized to a regular 1 m grid cell size by taking the ordinary mean of all cell points.

4 Results

The neighbourhood size used for surface normal estimation influences the level of detail of the skeleton. Larger neighborhoods reduce the ability to capture small landforms, but tighter neighborhoods risk to overfit insignificant morphologies or even noise. As we rasterize point clouds into DTMs, a neighborhood size of 4 is used, meaning that only the grid cells neighboring in X and Y direction are used to fit a plane for surface normal estimation.

4.1 Sand engine

The MAT settings for the Sand engine dataset are as follows. The initial radius is set at 50 m, while the values of the denoising parameter and the planarity parameter were both 10°. These settings are based on an empirical analysis of initial results.

Figure 6 shows for epochs S1, S3 and S5 the estimated ridge points, in red, superimposed on a hillshaded DTM. Epochs S2 and S4 show similar results to epochs S3 and S5, respectively. Epoch S1 shows elongated features, which can be interpreted as wind tails. These elongated features are visible both in the hillshade and in the ridge lines. In epoch S3 these elongated features have largely disappeared. The estimated ridge lines have shrunk accordingly, as only rounded dune tops remain. Epoch S5 shows two regimes. On the top left, rounded dune tops and short ridges prevail, which aligned with the results from epoch S3. A contrasting pattern is visible at the bottom. Here, the ridge lines are more simlar to the ridge lines in epoch S1, and are parallel to a deeper gully, oriented SW-NE.

Figure 7, A) provides, for each of the five epochs, the orientation of the MAT derived ridge points. In the circular plots, both the dip directions (in red) and the strike angles (in blue) are visualized. The dip direction provides the direction perpendicular to the morphology, while the strike angles give the direction of the ridge lines. Figure 7, B) summarizes the wind conditions for the period proceeding each of the UAV LiDAR acquisition as indicated.

Epoch S1 was apparently proceeded by a period of stronger winds from South West direction. It seems that, as a consequence, the juvenile dune field MAT strike aligned itself parallel to the wind. The stronger wind may have enabled sand transport. Once the wind reached the lee side of a dune head, wind strength may slightly drop, resulting in sedimentation at the lee side. If such process is able to continue for a while, elongated dune ridges parallel to the wind direction can develop.

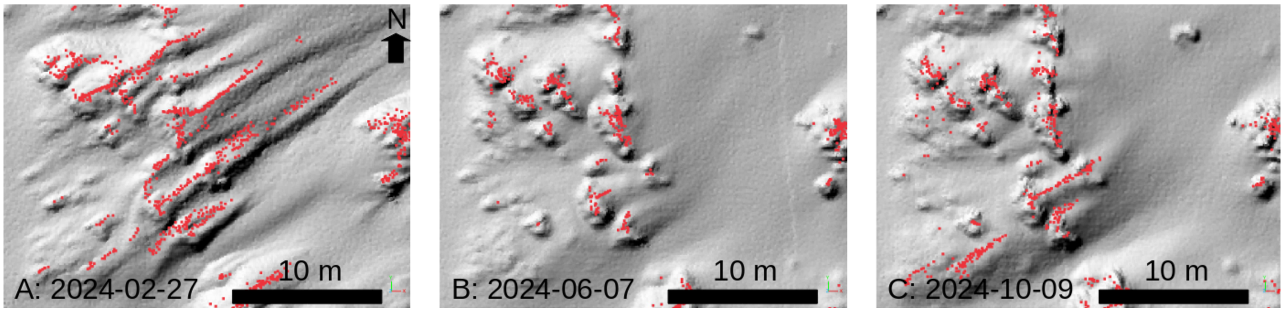

Figure 6. MAT points projected on hillshade visualization of UAV LiDAR DTMs for A), epoch S1, B) epoch S3, and C), epoch S5, at an embryo dune field at the Sand engine.

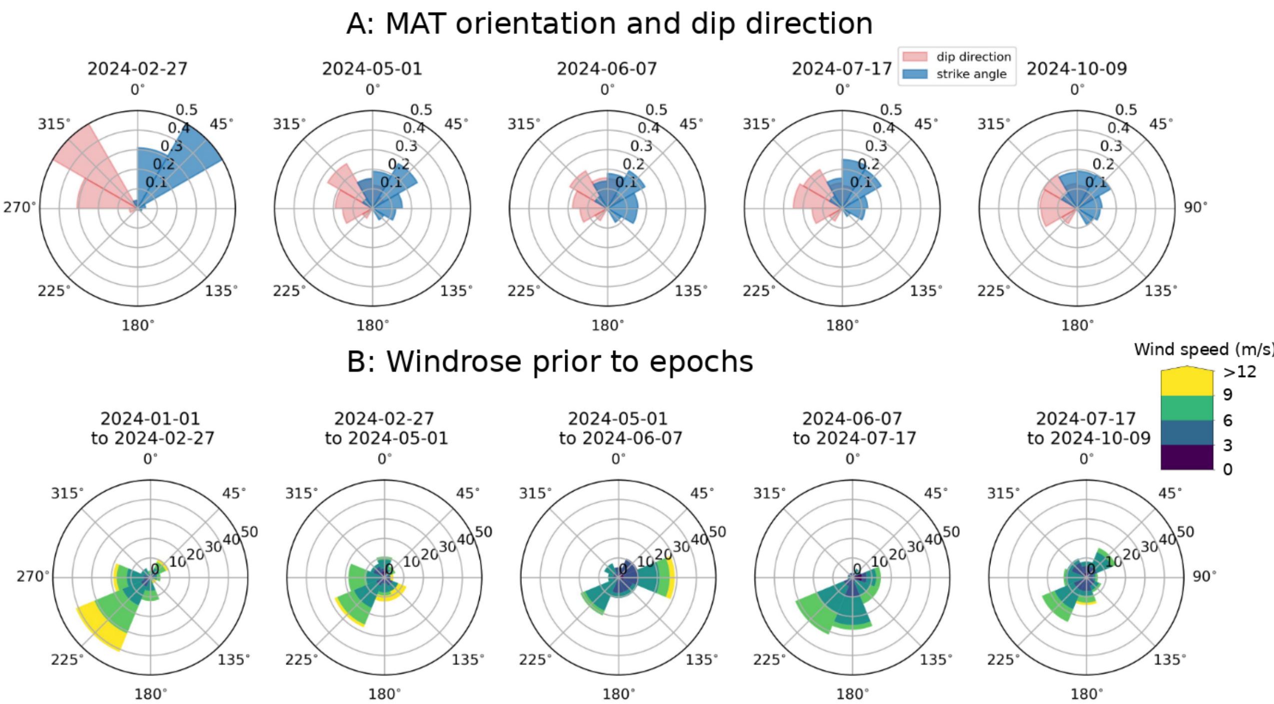

Figure 7. A) Distribution of orientation of vertically projected Internal Medial Axis Transform (MAT) points based on local neighborhood. The strike angle represents the azimuth direction of the longest axis of the ridge. The dip direction refers to the direction in which the MAT plane slopes, corresponding to Figure 2. The latter is symmetrically ambiguous for vertical MAT surfaces, and as such all were computed in one direction. B) Wind rose of the wind regime during periods as indicated, prior to each epoch. The radial axis represents the percentage of time a certain interval of wind speed was present.

Prior to epochs S2 and S3, see Figure 6, B), winds were weaker and more variable in direction. Previous leeward tails of both ridges and gullies have largely disappeared, and the area behind the dune fronts has flattened out. Before epoch S4, Figure 6, C), wind has a predominantly SW orientation, but wind speeds do not exceed 9 m/s. Gullies and tails with the same SW orientation are present at the bottom of the figure, but less pronounced than at epoch $S1$, while ridges at the top of the figure are largely similar to the situation in epoch $S1$.

4.2 Pila

The MAT settings for the Pila dataset are as follows. The initial radius is 200 m, the denoising and planarity parameter angles were both set to 20°. These settings are based on an empirical analysis of initial results.

Figure 3 illustrates the actual dip across the Pila dune. One can see the overall oblique MAT surface across two ridges. The top of the MAT surface is slightly curved: smaller dip values correspond to a

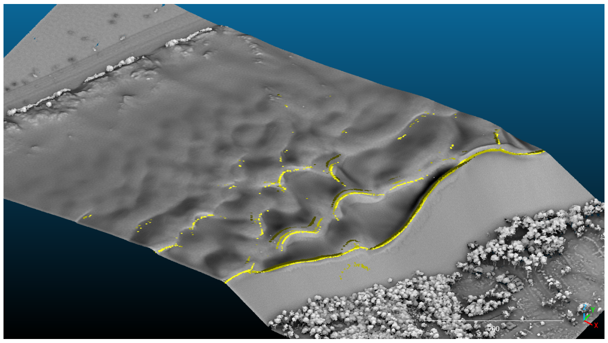

Figure 8. MAT ridge points (radii between 50 and 60 m) of epochs $P1$ (dark), $P2$ and $P3$ (light) projected on ALS Pila topography of 30 Sept. 2023.

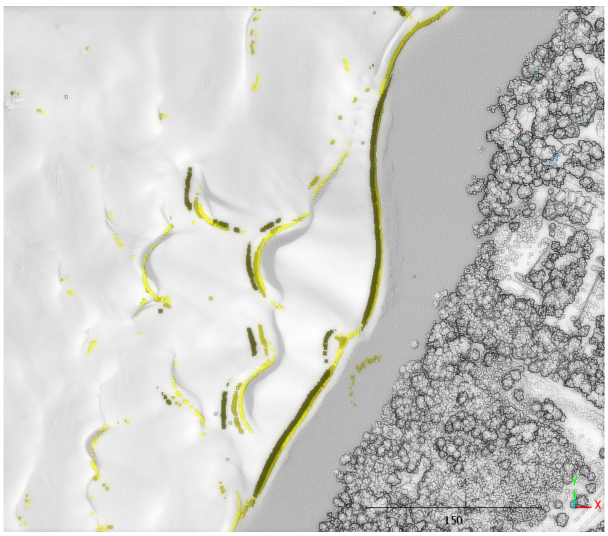

Figure 9. MAT ridge points for epochs $P1$, $P2$ and $P3$, overlaid on ALS LIDAR dune field for Pila.

shorter radius.

Figure 8 shows the extracted ridge points for epoch $P1$, overlaid on a shaded relief terrain model. Note that in this case the ridge points are MAT points projected onto the surface using a local MAT neighborhood as discussed in Section 2.4. As can be seen, the projected MAT points are indeed located on the ridges as visible in the shaded relief plot, but some systematic deviations occur. A possible explanation is that involving a MAT neighborhood has a smoothing effect, which keep projected ridge points away from the real ridge locations. This has to be analyzed further though. An alternative explanation is that the peaks of the dunes display a different morphology than the full dune, that is, the dune top may have a more direct response to the forcing.

Figure 9 has the extracted ridge points for all three

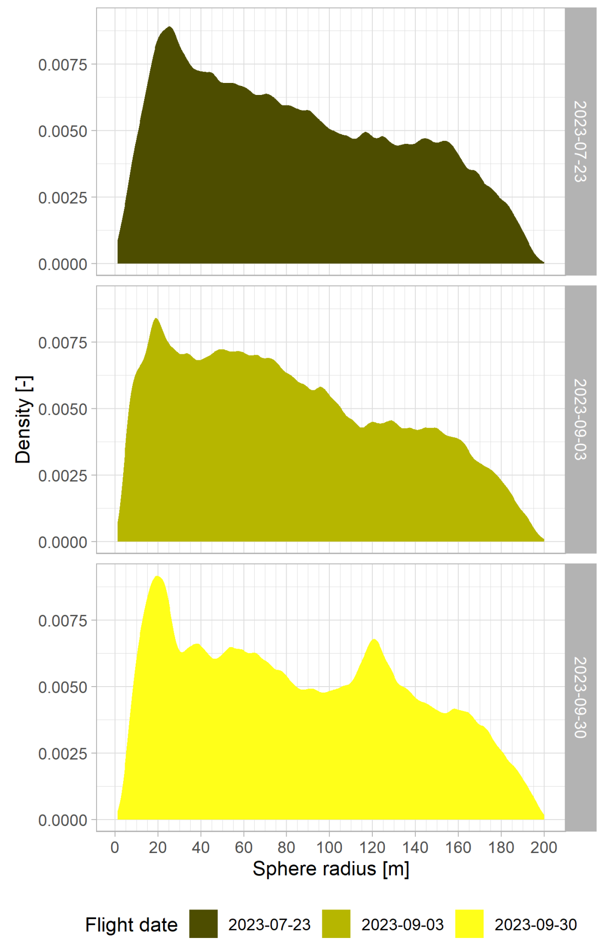

Figure 10. Histograms of the MAT radii values for Pila. Note the density changes in the range between 40 and 120 m between epochs

epochs $P1$, $P2$ and $P3$ superimposed on $P3$ shaded relief DTM. In addition, Figure 10 shows three histograms, one for each epoch P1, P2 and P3, respectively with identical temporal color coding. The histograms summarize MAT sphere radii distribution at each epoch. Here bigger radii of up to 200 m correspond to broader dune ridges. Histograms all display a similar mode with sphere radii around 20 m. But from July to September longer radii morphologies emerge. At the end of September (P3) a remarkable secondary mode emerges for feature matching spheres radii of ca. 120 m. Figure 9 shows that the dominant ridge line to the east remains relatively stable through the summer 2023 (see also Figure 3), and that secondary ridges have drifted landward at a rate of ca. 9 m in 67 days, i.e. $0.13 m/day$.

5 Conclusions

The Medial Axis Transform (MAT) with its accompanying parameters is a morphological shape descriptor that can be used to effectively describe and monitor the shape of dynamic landscape elements such as dunes. In this contribution it is shown how a robust version of the shrinking ball algorithm can be used to estimate ridge points, and proxies for dune size and dune asymmetry from two types of LiDAR data. On a juvenile dune field sampled by UAV-LiDAR the MAT method was demonstrated to be able to quantify quick morphological response from changing wind conditions. On the mature Pila dune, sampled by airborne LiDAR, the MAT method was able to automatically reveal changes in secondary dune ridges, and suitable to analyze the size and asymmetry of dune ridges. Further research is needed to study the sensitivity of the method to parameter settings such as the local MAT neighborhood size.

Acknowledgements

This research has been partly supported by the Netherlands Organization for Scientific Research (NWO, grant no. 20014) as part of the Open Technology Programme.

References

Blum, H. (1967). A transformation for extracting new descriptions of shape. *Models for the perception of speech and visual form*, pages 362–380.

Bossard, V. and Nicolae Lerma, A. (2020). Geomorphologic characteristics and evolution of managed dunes on the South West coast of France. *Geomorphology*, 367:107312.

Chen, K., Wang, C., Lu, M., Dai, W., Fan, J., Li, M., and Lei, S. (2023). Integrating topographic skeleton into deep learning for terrain reconstruction from GDEM and Google Earth image. *Remote Sensing*, 15(18).

Daynac, J., Bessin, P., Pochat, S., Mourgues, R., and Shumack, S. (2024). A new workflow for mapping dune features (outline, crestline and defects) combining deep learning and skeletonization from DEM-derived data. *Geomorphology*, 463:109369.

Grohmann, C. H., Garcia, G. P., Affonso, A. A., and Albuquerque, R. W. (2020). Dune migration and volume change from airborne LiDAR, terrestrial LiDAR and Structure from Motion-multi view stereo. *Computers & geosciences*, 143:104569.

Hulskemper, D., Anders, K., Antolínez, J., Kuschnerus, M., Höfle, B., and Lindenbergh, R. (2022). Characterization of morphological surface activities derived from near-continuous terrestrial lidar time series. *ISPRS Archives*, 48(2/W2-2022):53–60.

IGN (2025). LiDAR HD - une cartographie 3d du sol et du sursol de la France. https://geoservices.ign.fr/lidarhd, last visited: February 5, 2025.

Kuschnerus, M., Lindenbergh, R., and Vos, S. (2021). Coastal change patterns from time series clustering of permanent laser scan data. *Earth Surface Dynamics*, 9(1):89–103.

Ma, J., Bae, S. W., and Choi, S. (2012). 3D medial axis point approximation using nearest neighbors and the normal field. *The Visual Computer*, 28:7–19.

Peters, R. (2018). Point cloud modelling with the 3D medial axis transform. Project website, https://3d.bk.tudelft.nl/projects/3dsm/, last visited: February 5, 2025.

Peters, R. and Ledoux, H. (2016). Robust approximation of the medial axis transform of LiDAR point clouds as a tool for visualisation. *Computers & Geosciences*, 90:123–133.

Stive, M. J., De Schipper, M. A., Luijendijk, A. P., Aarninkhof, S. G., van Gelder-Maas, C., Van Thiel de Vries, J. S., De Vries, S., Henriquez, M., Marx, S., and Ranasinghe, R. (2013). A new alternative to saving our beaches from sea-level rise: The sand engine. *Journal of Coastal Research*, 29(5):1001–1008.

Walker, I. J., Eamer, J. B., and Darke, I. B. (2013). Assessing significant geomorphic changes and effectiveness of dynamic restoration in a coastal dune ecosystem. *Geomorphology*, 199:192–204.

Widyaningrum, E., Peters, R. Y., and Lindenbergh, R. C. (2020). Building outline extraction from als point clouds using medial axis transform descriptors. *Pattern Recognition*, 106:107447.